Radiocarbon, Vol 59, Nr 1, 2017, p 69–89 DOI:10.1017/RDC.2016.107

VEGETATION CHANGE IN SOUTHWESTERN AMAZONIA (BRAZIL) AND RELATIONSHIP TO THE LATE PLEISTOCENE AND HOLOCENE CLIMATE

Dilce F Rossetti[1*] • Marcelo C L Cohen[2] • Luiz C R Pessenda[3]

[1]Instituto Nacional de Pesquisas Espaciais, Observação da Terra. São José dos Campos 12245-970- SP, Brazil.
[2]Universidade Federal do Pará, Centro de Geociências. Belém 66075-900-PA, Brazil.
[3]Universidade de São Paulo, Laboratório de Carbon-14. Piracicaba 13416-000-SP, Brazil.

ABSTRACT. The Late Quaternary climate in Amazonia is an issue still open to debate, with hypotheses varying from alternate dry and wet episodes to stable climate with undisturbed rainforest. We approach this question using $\delta^{13}C$, C/N, and, to a lesser extent, $\delta^{15}N$ from deposits derived from four cores, with the results combined with published pollen data from two of these cores. These data were analyzed within the context of radiocarbon dating, which revealed ages ranging from 42.8–41.8 to 2.3–2.2 cal ka BP. Fluvial channel and floodplain deposits with freshwater phytoplankton recorded a trend of wet climate with dry episodes before ~40 cal ka BP, followed by humid and cold climate until the Last Glacial Maximum, with intensified aridity towards the end of the Late Pleistocene. Peaks of increased contributions in C_4 land plants in the mid- to late Holocene were not synchronous and have no correspondence with Amazonian Holocene dry episodes, being due to sedimentary processes related to fluvial dynamics during the establishment of herbaceous fields on abandoned depositional sites. Thus, the climate remained wet in the Holocene, which would have favored the expansion of the Amazonian rainforest as we see today.

KEYWORDS: carbon isotopes, vegetation, Late Pleistocene–Holocene, southwestern Amazonia, climate, sedimentary dynamics.

INTRODUCTION

Since its origin in the Miocene (Duarte 2003), the distribution of the Amazonian rainforest has changed, most likely due to climate fluctuations. However, this hypothesis remains open to debate, including the question of how the rainforest behaved under the impact of Pleistocene–Holocene glacial/interglacial events. Savanna corridors were proposed during dry or cold climates of the Last Glaciation (LG) (van der Hammen and Hooghiemstra 2000). Forest contraction and expansion due to glacial/interglacial fluctuations have also been proposed (Haffer 1969; Liu and Colinvaux 1985; Bush et al. 1990; Colinvaux et al. 1996; Ledru 2002; Ledru et al. 2006). During the Last Glaciation Maximum (LGM), the humidity was reduced 20–55% and the temperature was between 2° and 6°C below modern values (van der Hammen and Absy 1994; van der Hammen and Hooghiemstra 2000; Cohen et al. 2014). Additionally, several climatic changes are documented in the Holocene, as a response of the El Niño/Southern Oscillation (ENSO) (Martin et al. 1993, 1997) and migration of the Intertropical Convergence Zone (Servant et al. 1981; Absy et al. 1991; Behling 1996; Sandweiss et al. 1996, 1999; Behling and Costa 2000; Bush et al. 2000; Mayle et al. 2000; Weng et al. 2002; Burbridge et al. 2004).

The majority of the Amazonian climatic data indicates alternating dry (grassland) and wet (forest) episodes, based on pollen from a few sites (e.g. Absy et al. 1991; van der Hammen and Absy 1994; Colinvaux et al. 2000; Mayle et al. 2000), and, to an even lesser extent, eolian paleodunes (Carneiro Filho et al. 2002). Several misleading interpretations may arise when these data are analyzed. For instance, although cold/dry episodes are mostly based on records of ^{14}C grasses, this vegetation type is presently distributed over large areas of the Amazonian ecosystem; thus, its past occurrence cannot be directly related to dry climate (e.g. Colinvaux et al. 2001). The Amazonian paleodunes also should not be used as a proxy for dry climate, as they are not synchronous and may have a geomorphological, rather than

*Corresponding author. Email: rossetti@dsr.inpe.br.

climatic, origin (Teeuw and Rhodes 2004; Latrubesse and Franzinelli 2005). Thus, there is a need to conduct investigations on the Late Pleistocene–Holocene Amazonian climate and also to critically analyze the suitability of techniques that have been applied in these reconstructions.

With a few exceptions (see e.g. Cohen et al. 2014), most of the Amazonian sedimentary deposits have low potential for pollen preservation due to oxidizing conditions; thus, it is important to consider alternative proxies for reconstructing the paleoclimate in this region. $\delta^{15}N$ and $\delta^{13}C$ analyses provide information on sources and relative quantities of organic material in continental sedimentary deposits, being arguably useful in paleoclimatic reconstructions (Meyers 1994, 1997; Thornton and McManus 1994; Cloern et al. 2002; Ogrinc et al. 2005). $\delta^{15}N$ values around 10.0‰ or higher and around 0‰ are usually related to aquatic and terrestrial plants, respectively (Thornton and McManus 1994; Meyers 1997), although the controls on N cycling in sediments and soils are not completely understood yet, particularly considering the wide range of ecosystems with varying sources and fractionation pathways over time (e.g. Wang and Macko 2011; Vitousek et al. 2013; Craine et al. 2015). Soil degradation may also lead to ^{13}C enrichment (e.g. Chikaraishi and Naraoka 2006; Garcin et al. 2014; Schwab et al. 2015), but the C pathway in the ground is reasonably better known (Premuzic et al. 1982; Meyers 1994; Sifeddine et al. 2001; Rommerskiechen et al. 2006; Diefendorf et al. 2011; Sinninghe Damsté et al. 2011). In particular, recent developments on this issue based on organic chemistry analysis of biomarkers, such as long-chain *n*-alkali lipids, confirmed that the $\delta^{13}C$ values from sedimentary organic matter are within the range of $\delta^{13}C$ values of plants (Garcin et al. 2014), which favors the use of this proxy in paleoecological reconstructions. Disregarding plant types with a crassulacean acid metabolism (CAM) carbon fixation pathway, C_3 and C_4 land plants growing under atmospheric CO_2 concentration of about 330 ppm ($\delta^{13}C$ of –7‰) show $\delta^{13}C$ values between –33.0‰ and –23.0‰, and –15.0‰ and –9.0‰, respectively (Deines 1980). Because the $\delta^{13}C$ land plants may overlap with those from aquatic plants, the isotopic ratio must be used with C/N for discriminating freshwater phytoplankton (C/N = 4.0 to 10.0) (Meyers 1994) from land plants (C/N ≥ 12.0) (e.g. Cloern et al. 2002; Wilson et al. 2005).

In the present work, we used an integrated approach comprising analyses of $\delta^{13}C$ and C/N, geomorphology, sedimentology, and accelerator mass spectrometry (AMS) ^{14}C chronology for estimating changes in vegetation patterns during the Late Pleistocene and Holocene in a marginal area of the Madeira River, southwestern Amazonia, dominated by fluviatile deposits (Figure 1). The area was chosen based on its location in a forested terrain with large incidence of open vegetation. The goal was to determine when large areas of open vegetation (grassland) developed within the dense forest and what was the main factor controlling the changes in vegetation patterns through time. Modern grasslands in this area were previously attributed to the heritage of early- to mid-Holocene drier climates (e.g. Freitas et al. 2001; Pessenda et al. 2001, 2004, 2005). However, these studies based their interpretations only on a few $\delta^{13}C$ soil data, which do not allow the distinction, for instance, between C_4 land plants and C_4 freshwater phytoplankton, the latter being also present in many standing water bodies of the Amazonian wetlands (Amorim et al. 2009). The present study analyzes $\delta^{13}C$ and C/N data within a geomorphological, sedimentological and ^{14}C context. Despite the limitations, we also tested the application of $\delta^{15}N$ values for differentiating land (~0‰) and aquatic (10‰ or higher) plants, as commonly used in the literature (e.g. Thornton and McManus 1994; Meyers 1997), and compared these results with C/N variations along the studied profiles. The larger body of information presented herein provides new insights for accessing available climatic

https://doi.org/10.1017/RDC.2016.107 Published online by Cambridge University Press

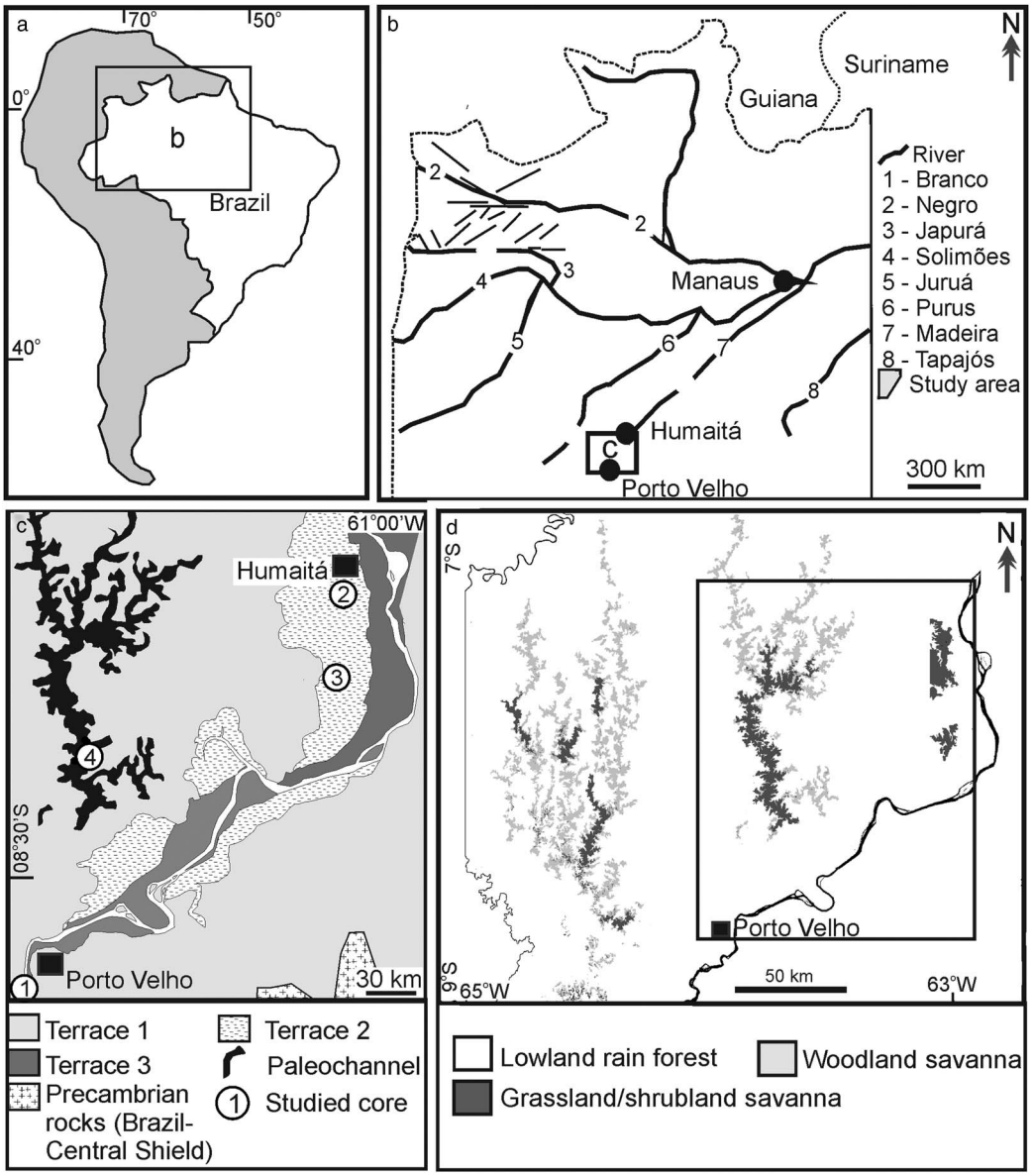

Figure 1 (a,b) Location of the study area between Porto Velho and Humaitá, southwestern Amazonia, Brazil (a), with indication of main river systems and tectonic lineaments (b). (c) Study area with location of fluvial terraces and the four studied cores (modified from Rossetti et al. 2014). (d) Main vegetation types in the study area. Inner box indicates the study area shown in Figure 1c.

interpretations from the study area, advancing the discussion about the effect of climate oscillation associated with the last glaciation in southeastern Amazonia.

PHYSIOGRAPHY AND GEOLOGICAL FRAMEWORK

The study area is located between the city of Porto Velho in the north of the State of Rondonia and the town of Humaitá in the south of the State of Amazonas (Figure 1a,b). Climate in this

https://doi.org/10.1017/RDC.2016.107 Published online by Cambridge University Press

region is characterized by short dry seasons (Am in Köppen's classification) and a mean annual temperature of 28°C, with a minimum of 10°C in June and July. Precipitation averages 2500 to 3000 mm/yr and the relative humidity is 85%. Vegetation is chiefly arboreal, including lowland *Ombrophyla* forest in sharp contact with large patches of open vegetation, mostly grassland and shrubland (Figure 1d) (Radambrasil 1978).

Geologically, the study area is within the Solimões Basin, which is a 600,000-km² intracratonic Paleozoic rift that evolved into a foreland basin in the Cretaceous and Cenozoic due to intraplate extension and tectonic uplifts in the Andean Chain. Cenozoic deposits in this basin consist of the Solimões and Içá Formations (Cunha et al. 1994), as well as unnamed Pleistocene–Holocene deposits (Rossetti et al. 2005). In the study area, the latter deposits consist of three tectonically influenced fluvial terraces formed before 43,500 and 31,696–32,913 cal yr BP (terrace T1), between 25,338–26,056 and 14,129–14,967 cal yr BP (terrace T2), and between 12,881–13,245 to 3158–3367 cal yr BP (terrace T3) (Rossetti et al. 2014; Figure 1c).

MATERIALS AND METHODS

This study was based on four continuous cores of up to 10 m long each (Figure 1c), acquired with a percussion drilling Robotic Key System (RKS), model COBRA mk1 (COBRA Directional Drilling Ltd., Darlington, UK). Cores 2 and 4 are novel, while cores 1 and 3 correspond respectively to the cores designated as HU-1 and PV02 in a previous publication (Cohen et al. 2014). The two latter cores were included in the present work because these authors focused only on pollen data, having provided no detailed analysis of isotope data or facies interpretation. Facies analysis was based on measured lithostratigraphic profiles containing information such as lithology, texture, sedimentary structure, and type of contact. The description of various fluvial paleomorphologies was based on the analysis of remote sensing data including Landsat 5 – TM images (www.dgi.inpe.br) and a digital elevation model (DEM) from the Shuttle Radar Topography Mission (SRTM) (ftp://e0srp01u.ecs.nasa.gov/srtm/). The optical images were registered and processed for R (red), B (blue), G (green) band composition. The SRTM – DEM consisted on the C-band original 90-m resolution (3 arc seconds) obtained with synthetic aperture radar. The SRTM data were processed using customized shading schemes and palettes in the Global Mapper Software 2009 in order to highlight the features of interest. High-resolution QuickBird and SPOT optical images from Google Earth helped in analyzing the paleomorphologies in more detail and establishing their relationship to vegetation cover.

For the total organic carbon (TOC), total nitrogen (TN), and isotope analyses, 76 core samples were systematically collected at 20-cm intervals along the studied cores. Homogenized bulk samples were oven-dried at 50°C for 48 hr. A parcel (~1 g) of each sample was acidified with 1.5M HCl and left overnight to allow inorganic carbon to be liberated as CO_2. The samples were then repeatedly washed with distilled water to remove inorganic carbon and subsequently oven-dried at 60°C. The analyses were performed at the Nuclear Energy Center of Stable Isotopes and Agriculture Laboratory (CENA/USP). TOC and TN measurements were carried out on an elementary analyzer attached to a Mass Spectrometry ANCA SL 2020 of Scientific Europa. The results are expressed in % of dry weight for the total C and N. The isotopes ratios are provided in ‰ with respect to the VPDB (Viena Pee Dee Belemnite) standard for the $\delta^{13}C$ and atmospheric air for the $\delta^{15}N$, both with analytical precision greater than 0.2‰. Replicates were produced for every five samples analyzed. The C/N values represent the molar ratio between TOC and TN, calculated based on the following equation: $C/N_{molar} = (\%TOC/12.011)/(\%TN/14.007)$.

https://doi.org/10.1017/RDC.2016.107 Published online by Cambridge University Press

The chronological control was obtained from 22 samples of bulk sediments. Sampling did not follow a regular spacing, but it depended on the availability of fresh muddy sediments rich in organic carbon. The samples were collected aiming to record a succession of age variation with depth to each profile. Sample pretreatment and dating followed the Beta Analytic Radiocarbon Dating Laboratory (Miami, USA, lab code Beta-) standard technique for AMS dating. The pretreatment consisted of dispersing the sediment deionized water, followed by sieving through a 180-micron sieve to recover any available plant material and to remove any stones, gravels, or other course inorganic grains. The <180-micron size fraction was used in each case. Two 0.1N HCl baths were applied for 2 hr each at 70°C to remove any carbonates. Samples were rinsed to neutral and dried at 100°C for 12 hr, cooled, and weighed. After homogenizing with a mortar and pestle, a small portion of the sediment was tested under a microscope with 12M HCl to ensure complete removal of all carbonate. Each sample was subsampled and combusted to CO_2 in a closed chemistry line, which had been purged of any CO_2 to a level below $10e^{-15}$ atoms (background levels). The CO_2 was then introduced into a reaction vessel containing an aliquot of cobalt metal catalyst. Hydrogen was introduced such that when the cocktail was heated to 500°C, the CO_2 cracked to carbon (graphite). The graphite was pressed into a target for measurement in the AMS. The AMS was calibrated to provide an accurate ratio of the $^{14}C/^{13}C$ ratio between the sample graphite and a modern reference (NIST-4990C, oxalic acid). Quality assurance (QA) samples were reacted simultaneously in the chemistry lab and measured simultaneously in the AMS. The analytical result was obtained as a fraction of the modern reference, corrected for isotopic fractionation using $^{13}C/^{12}C$ ($\delta^{13}C$) and the ^{14}C age was calculated according to the convention of Stuiver and Polach (1977). The QA samples were checked for accuracy and observed to fall within expectations for the laboratory to accept and report the sample results. The QA acceptance was defined as the total laboratory error known to be within 2σ. The equipment used in these analyses was the Thermo Delta-Plus isotope ratio mass spectrometer ($\delta^{13}C$ precision of ±0.3‰) and a 250kV NEC single-stage particle accelerator (AMS precision of ±0.001–0.004 fraction modern). ^{14}C ages are reported in years before AD 1950 (yr BP) normalized to a $\delta^{13}C$ of –25‰VPDB and in cal yr BP according to SHCal13 (Reimer et al. 2013). The software CALIB v 7.1 html was used for age calibration.

RESULTS

Morphological Context and Sedimentology

The studied cores were acquired along fluvial terraces at the margin of the Madeira River (Figure 1c). These terraces have altitudes ranging from 100–85 m (oldest), 85−65 m, and 65−45 m (youngest), the latter located closer to the modern river valley. Core 1 stands at an altitude of 57 m, being inserted in the lowermost fluvial terrace (T3) less than 300 m from the margin of the modern Madeira River (Figure 2a). Vegetation in this site consists of seasonally flooded *Ombrophyla* forest. Core 2 occurs at an altitude of 67 m over the second fluvial terrace (T2) (Figure 2b–d). The southern part of this terrace contains a large paleomeander belt nearly 2.5 km wide (Figure 2b,c), which is covered in part by grassland and in part by *Ombrophyla* dense alluvial forest (Figure 2c,d). Core 2 was plotted in a grassy floodplain located northeastward of the paleomeander (Figure 2d). Core 3 (Figure 2b,e) is also located in an area of open vegetation corresponding to a paleomeander of terrace T2. Core 4 is located at 79 m altitude in an area of open vegetation corresponding to a paleochannel in the uppermost (oldest) terrace (i.e. T1) of the Madeira River (Figure 2f,g).

The cores consist of sandy and muddy lithologies, with cores 1 and 2 being the muddiest ones and core 4 the sandiest one. Three facies associations are present, hereafter designated as FAA,

https://doi.org/10.1017/RDC.2016.107 Published online by Cambridge University Press

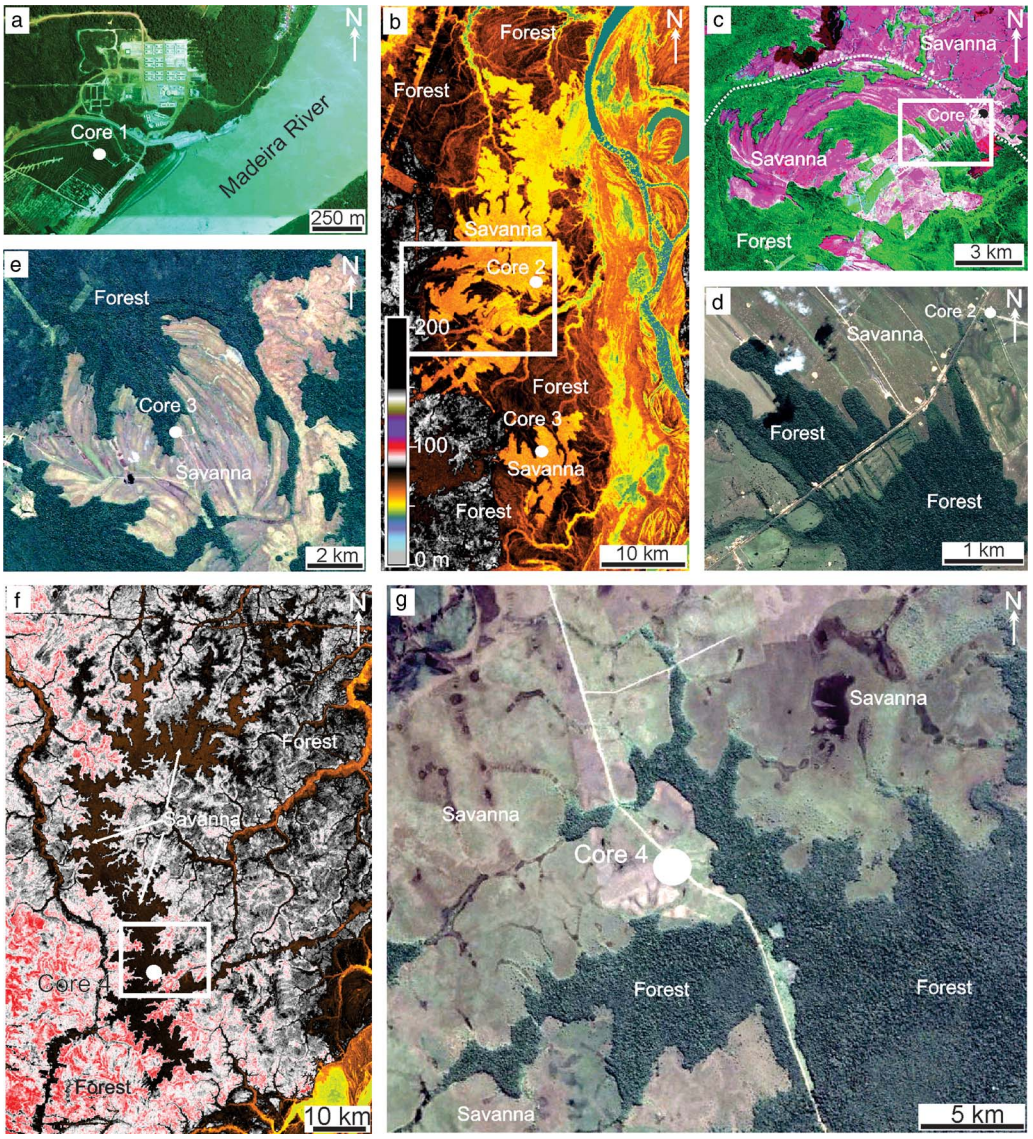

Figure 2 Geomorphological context of the studied cores. (a) Core 1 located in a primarily seasonally flooded area (now anthropogenically-modified nonforested area) located in the lowest fluvial terrace of the Madeira River (QuickBird image, Image 2007–Digital Globe). (b) DEM–SRTM locating two large savanna patches over an intermediate terrace of the Madeira River, where cores 2 and 3 were plotted. Note that the first core occurs in a large savanna area corresponding to a floodplain paleoenvironment, and the second one in a savanna area developed over a paleomeander. (c,d) Landsat (c) and QuickBird image (Image 2007–Digital Globe) (d) with detailed view of the paleomorphology and floristic composition in the areas corresponding to cores 2 and 3. Note in (c) the semi-circular shape with several concentric lines corresponding to a paleomeander in sharp contact (hatched line) with its associated paleofloodplain. Note also the sharp contrasts between savanna (pink) and forest (green) (colors correspond to the online color version of the article); (e) Detail of the site of core 3, acquired also over a paleomeander displaying several concentric lines representative of channel migration through time (QuickBird image, Image 2007–Digital Globe). (f) DEM–SRTM illustrating the place where core 4 was acquired. Note that this core was plotted over a large, elongated belt of savanna, which highlights a southward trending paleodrainage system. (g) Detailed view of site 4, illustrating the floristic types (QuickBird image, Image 2007-Digital Globe).

https://doi.org/10.1017/RDC.2016.107 Published online by Cambridge University Press

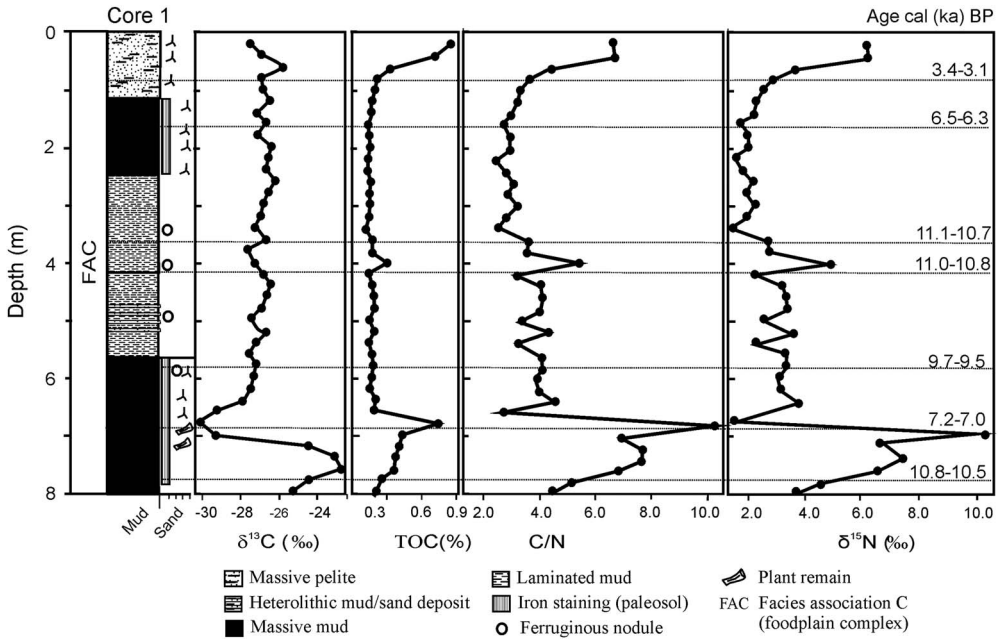

Figure 3 Litostratigraphic profile of core 1, with the vertical distribution of sedimentary facies, depositional environments, ages, $\delta^{13}C$, $\delta^{15}N$, and C/N. Note that ages are cal (ka) BP.

FAB, and FAC, which correspond respectively to the following paleoenvironments: active channel, abandoned channel, and floodplain complex (Figures 3–6).

FAA is up to 4 m thick, occurs only in cores 3 and 4, and is characterized by sharp erosional bases mantled by cross-stratified sandstone that grade upward into massive sandstone. The base of FAA in core 3 was not reached. The lithologies form fining-upward successions varying upward from medium/coarse-grained sandstone to very fine-grained sandstone, which are moderately to well sorted and mostly composed of quartz grains.

FAB, also restricted to cores 3 and 4, grades upward from FAA and is up to 3 m long in core 4 and only 0.6 m in core 3. Deposits in FAB consist of three lithofacies: very fine- to fine-grained massive sandstone, parallel-laminated mudstone, and heterolithic deposits. The latter includes mudstone with lenses of silty or very fine- to medium-grained sandstone internally massive or trough cross-laminated; undulating silty and very fine- to medium-grained sandstone interbedded either with laminated or massive mudstone; and mudstone lenses within fine- to medium-grained sandstone. These lithofacies configure fining-upward successions.

FAC is recorded in all cores, being more expressive in cores 1 and 2. This association occurs on top of FAB in cores 3 and 4, completing its overall fining-upward nature. The lithologies consist of parallel-laminated mudstone that grades upward into indurated massive mudstone and pelite with roots and/or root marks. Organic plant debris are present and iron oxides/hydroxide nodules (a few mm in diameter) are dispersed in these deposits. Thin (i.e. up to 0.3 m thick) beds of massive silty to very fine-grained sandstone are also present and they grade downward from parallel-laminated mudstone and lenticular heterolithic deposits forming coarsening-upward successions. Alternatively, sandy layers are interbedded with laminated mudstone as rhythmites.

https://doi.org/10.1017/RDC.2016.107 Published online by Cambridge University Press

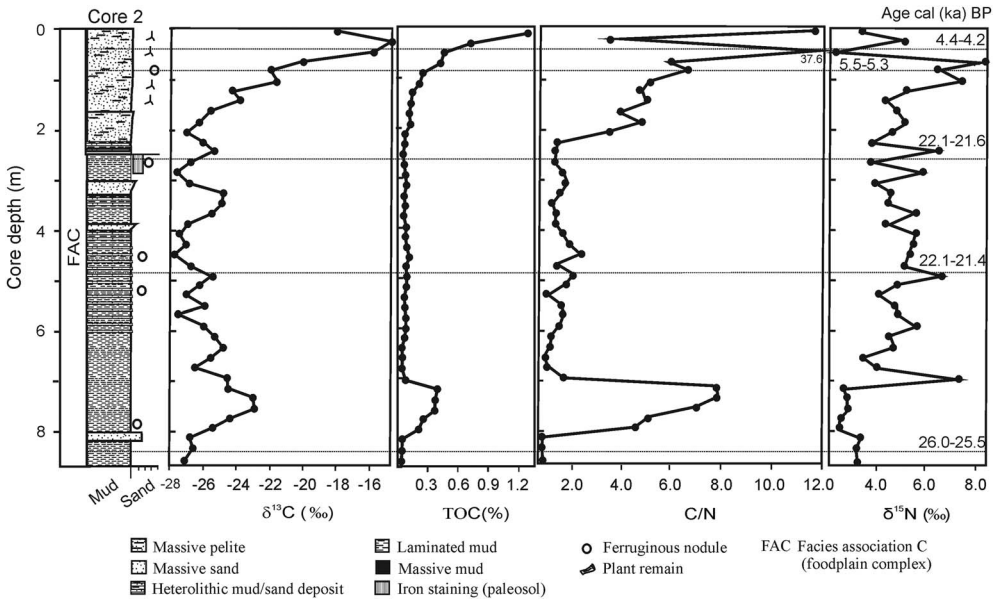

Figure 4 Litostratigraphic profile of core 2, with the vertical distribution of sedimentary facies, depositional environments, ages, $\delta^{13}C$, $\delta^{15}N$, and C/N. Note that ages are cal (ka) BP.

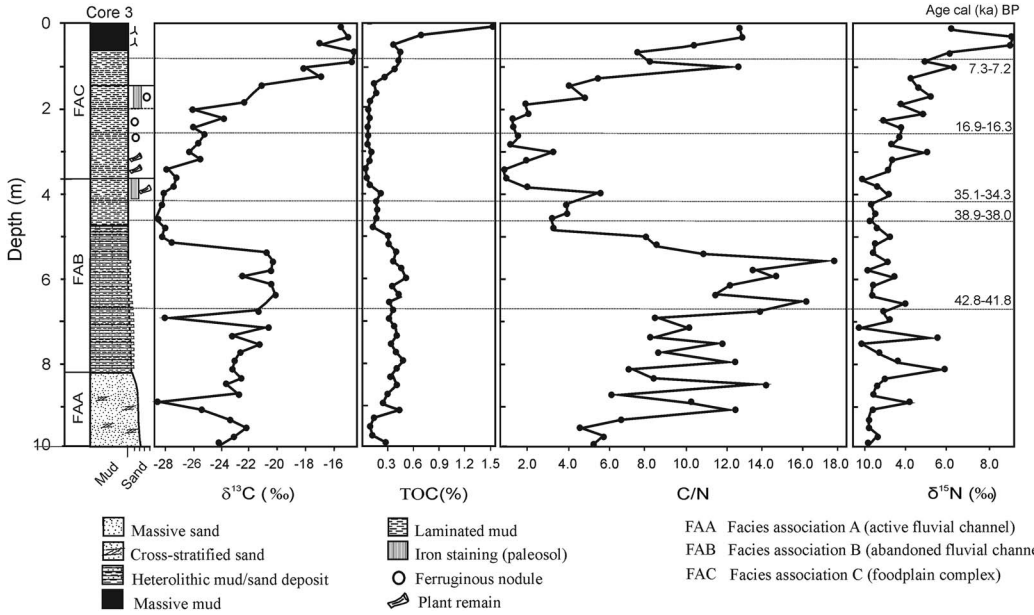

Figure 5 Litostratigraphic profile of core 3, with the vertical distribution of sedimentary facies, depositional environments, ages, $\delta^{13}C$, $\delta^{15}N$, and C/N. Note that ages are cal (ka) BP.

Radiocarbon Chronology

^{14}C analyses of the studied deposits (Table 1) revealed Late Pleistocene and Holocene ages ranging from 42.8–41.8 to 2.3–2.2 cal ka BP. The lower half of core 3 recorded the oldest ages (i.e. 42.8–41.8 to 35.0–34.3 cal ka BP). Upward, these deposits displayed a paleosol horizon that

https://doi.org/10.1017/RDC.2016.107 Published online by Cambridge University Press

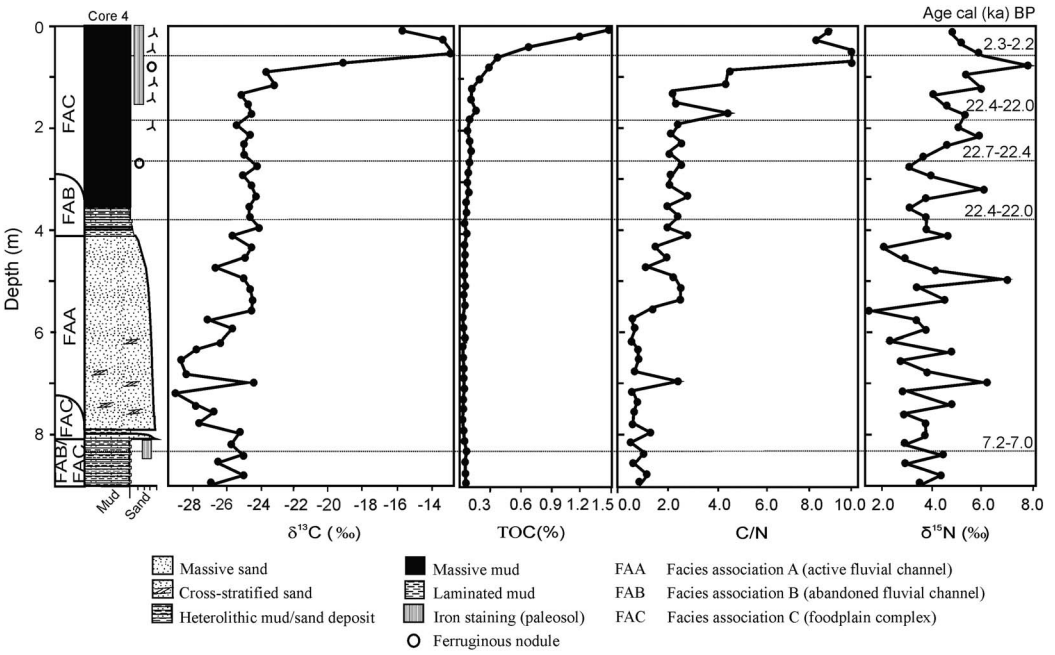

Figure 6 Litostratigraphic profile of core 4, with the vertical distribution of sedimentary facies, depositional environments, ages, $\delta^{13}C$, $\delta^{15}N$, and C/N. Note that ages are cal (ka) BP.

Table 1 Radiocarbon ages of the studied deposits.

Core	Lab code (Beta-)	Coordinates	Depth (m)	^{14}C yr BP	cal yr BP 2σ
1	288714	8°34′08″S, 63°43′48″W	0.8–0.9	3050 (±40)	3349–3093
	406678		1.6–1.7	5650 (±50)	6490–6296
	285259		3.6–3.7	9590 (±50)	11,108–10,694
	304790		4.0–4.1	9700 (±50)	11,034–10,783
	406679		5.8–5.9	8700 (±30)	9689–9540
	296243		6.8–6.9	6270 (±40)	7255–7005
	288715		7.8–8.0	9470 (±50)	10,788–10,508
2	406680	7°42′43″S, 63°05′32″W	0.4–0.5	3900 (±30)	4411–4218
	296244		0.8–0.9	4660 (±40)	5471–5277
	309797		2.6–2.7	18,100 (±70)	22,142–21,621
	285260		4.8–4.9	18,150 (±70)	22,067–21,394
	288716		8.3–8.4	21,450 (±130)	25,976–25,454
3	288718	7°55′26″S, 63°04′60″W	0.8–0.9	6310 (±30)	7271–7155
	288719		2.6–2.7	13,770 (±60)	16,863–16,316
	285261		4.0–4.1	30,800 (±170)	35,029–34,299
	304791		4.6–4.7	34,030 (±200)	38,944–37,952
	288720		6.7–6.8	38,130 (±360)	42,780–41,784
4	406683	8°06′02″S, 63°45′31″W	0.5–0.6	2250 (±30)	2329–2150
	288717		1.8–1.9	18,400 (±80)	22,431–21,954
	406684		2.6–2.7	18,680 (±70)	22,691–22,347
	406685		3.8–3.9	18,430 (±60)	22,443–22,007
	296246		8.2–8.3	6230 (±40)	7179–6957

https://doi.org/10.1017/RDC.2016.107 Published online by Cambridge University Press

indicates a hiatus, which was confirmed by the contrasting ages (i.e. 16.9–16.3 and 7.3–7.2 cal ka BP) of the overlying deposits. The second oldest age succession was recorded at 8.4–2.6 m of core 2, which varied upward from 26.0–25.5 cal ka BP to 22.1–21.4 cal ka BP. Similarly to core 3, this core also recorded a hiatus, with deposits above 2.6 m having ages of 5.5–5.3 and 4.4–4.2 cal ka BP. As expected by the location in the lowest terrace, the youngest age set was found in core 1, which varied from 11.1–10.7 to 3.4–3.1 cal ka BP in the last 4 m. Below this depth, three other ages were recorded from bottom to top, i.e. 10.8–10.6, 7.3–7.0, and 9.7–9.5 cal ka BP. This age succession recorded a time inversion. The presence of a palosol at these depths led to suggest that this may have occurred due to carbon rejuvenation by contamination with new carbon available when the sediments where subaereally exposed to pedogenesis (Figure 4). Core 4 showed continuous mud with ages ranging upward from 22.4–22.0 to 2.3–2.2 cal ka BP. However, a younger age of 7.2–7.0 cal ka BP was recorded at 8.3–8.2 m depth, which was also related to contamination by new carbon during pedogenesis.

Considering the provided calibrated ages, the sedimentation rates of the studied cores varied from about 0.2 (cores 3 and 4) to 0.3 (core 2) or up to 0.7 (core 1) mm yr^{-1}. These rates are presented only as a broad view on sedimentation rates, as these were calculated assuming that sedimentation remained constant through time, which may not be true in all instances.

Isotopic and Chemical Data

$\delta^{13}C$, $\delta^{15}N$, and C/N data varied largely, i.e. $\delta^{13}C$ = –30.1 to –14.6‰, $\delta^{15}N$ = 1.3 to 9.2‰, and C/N = 0.6 to 16.7 (Figures 3−6). The TOC and TN values were generally low in all cores, being <1.6% and 0.2%, respectively. These proxies displayed similar patterns of variation within and among individual profiles. Most of samples in core 1 (Figure 3) had $\delta^{13}C$ values of –28.9 to –22.9‰ and C/N values of 2.4 to 10.0. At 6.8 m depth, the C/N was as high as 10.0, the $\delta^{13}C$ was the most depleted (i.e. –30.1‰), while the $\delta^{15}N$ was as low as 1.3‰. Between 6.6 m and 4.2 m, the C/N (2.4 to 5.1) and $\delta^{15}N$ (2.6 to 3.7‰) increased, while $\delta^{13}C$ progressively enriched from –29.4 to –27.2‰. Above this depth, the $\delta^{13}C$ oscillated between –27.5 and –25.9‰, the C/N oscillated between 3.3 and 2.1, and then suddenly increased to 4.1 to 6.5 between 0.6 and 0.2 m depth, and the $\delta^{15}N$ progressively increased from 3.1 to 6.4‰.

Up to 4.2 m depth in core 2 (Figure 4), the $\delta^{13}C$ oscillated from –27.6 to –22.9‰, the C/N from 0.7 to 2.0, and the $\delta^{15}N$ from 3.2 to 7.2‰. An exception occurs between 8.0 and 7.2 m depth, where $\delta^{13}C$ was as depleted as –22.9‰, C/N was as high as 7.5, and $\delta^{15}N$ was as low as 2.6‰. Above 4.2 m depth, there was a progressive enrichment in $\delta^{13}C$, with sudden peak of –15.9‰ at 0.4 m depth, which was accompanied by an increase in C/N to 11.3 and a decrease in $\delta^{15}N$ to 2.5‰. Upward and after some oscillation, there was another remarkable peak of $\delta^{13}C$ enrichment to 18.6‰, while the C/N was as high as 37.6 and the $\delta^{15}N$ decreased from 5.0 to 3.3‰.

Core 3 (Figure 5) displayed the highest recorded range for all values, with $\delta^{13}C$ = –28.1 to –14.9‰, $\delta^{15}N$ = 1.8 to 9.2‰, and C/N = 0.9 to 16.7. The most striking finding is that, after several oscillations into depleted values, the $\delta^{13}C$ values were enriched to –14.59‰ at 2 m depth and upward. Below around 5.4 m depth, the $\delta^{13}C$ and C/N were highly oscillating, varying from –28.2 to –20.2‰ and 4.6 to 16.7, respectively. After several oscillations, the C/N had the lowest value (i.e. 2.0) at 3.8 m, increasing upward to 12.2. The marked change of $\delta^{13}C$ values from –20.9 to –16.9‰ at around 1.2 m depth is interesting, with this proxy remaining enriched upward. This enrichment in $\delta^{13}C$ coincides with increased C/N, which had peaks at 1 m depth of 11.5 and above 0.2 m depth of 12.2 to 12.1. Meanwhile, $\delta^{15}N$ progressively increased to a peak of 9.2‰, decreasing at the top to 6.2‰.

https://doi.org/10.1017/RDC.2016.107 Published online by Cambridge University Press

Values of $\delta^{13}C$, $\delta^{15}N$, and C/N along core 4 (Figure 6) were distributed more uniformly than in the previous cores, with a sudden change at 1.2 m depth. Hence, below 1.2 m, $\delta^{13}C$ was –28.0 to –24.2‰, with one value of –29.1‰ at 7 m, $\delta^{15}N$ is 1.6 to 7.0‰, and C/N is 0.6 to 2.7, with one value of 4.4 at 1.6 m. Above 1.2 m, the $\delta^{13}C$ values were enriched up to –15.56‰, while the $\delta^{15}N$ is 4.8–7.9‰, and the C/N is 4.3–9.2. At 0.6 m depth, the $\delta^{13}C$ varied from –23.5 to –19.6‰ and then –12.7‰ and the C/N varied from 4.4 to 9.1 and then 9.2, while $\delta^{15}N$ varied from 5.4 to 7.9‰.

DISCUSSION

Paleoenvironmental Evolution and Plant Contribution through Time

Our faciological and chronological data indicate that the studied cores contain sedimentary deposits typically accumulated in fluviatile environments during the last 43 ka BP. The $\delta^{13}C$, $\delta^{15}N$, and C/N values of these deposits allowed to infer changes in vegetation over this time interval. A prior consideration before using these proxies for this purpose is that these signals detected in the sedimentary record may differ from contemporaneous plants mostly due to one or a combination of the following factors: (i) biodegradation by aerobic microbes during and after sediment deposition (Thornton and McManus 1994; Cloern et al. 2002; see also references in Lamb et al. 2006 and Chen et al. 2008); (ii) biosynthesis of inorganic nitrogen (Meyers 1997; Chen et al. 2008); (iii) incorporation of different amounts of organic matter by various grain sizes (e.g. Keil et al. 1994); (iv) postdepositional chemical or biogenic modifications (see Chen et al. 2008 for a review); and (v) increased atmospheric CO_2 by ~20% since the LGM, which may affect the $\delta^{13}C$ values (Adams et al. 1990). Despite these potential interferences, a primary nature of the $\delta^{13}C$ and C/N values recorded in the study area is suggested by their non-random vertical distribution and good correspondence when deposits of similar ages are compared; many variations within a same facies association, indicating they are facies-independent; and the good agreement between plant types interpreted from these data and published pollen data from same profiles (see Cohen et al. 2014), as discussed below.

Previous works based only on $\delta^{13}C$ values of sedimentary deposits from the study area related changes from C_3 to C_4 land plants to directly alternating wet and dry phases (Pessenda et al. 1998, 2001, 2004, 2005). However, a comparison of data from the studied deposits with those from modern vegetation allowed detecting changes in vegetation types through time and also analyzing their potential causes considering the paleoenvironmental framework provided by facies analysis. For the discussion below, sedimentation rates were used to estimate ages in stratigraphic intervals lacking these data.

Our results indicated generally low C/N values (i.e. usually <12), which are more compatible with the prevalence of freshwater phytoplankton than land plants, the latter occurring only at certain stratigraphic intervals displaying C/N > 12. Both C_3 and C_4 land plants were present, with the first being recognized by $\delta^{13}C$ values comparable to those from a number of Amazonian trees, i.e. –37.8 to –25.9‰ (Ometto et al. 2006) or –37.8 to –28.9‰ (Francisquini et al. 2014) and also from modern soils of this region, i.e. usually < –27‰ (Magnusson et al. 2002).

The base of core 3, which corresponds to an uncertain age that approaches the limit of the ^{14}C dating technique, recorded the establishment of a fluvial channel. Although the basal channel surface was not reached in this core, this interpretation is provided by the upward gradation from FAA into FAB and FAC configuring a fining-upward succession, which matches with descriptions of many channel deposits (e.g. Atchley et al. 2004; McLaurin and Steel 2007). Sand was formed at the bottom of this channel for a certain period of time. However, before

https://doi.org/10.1017/RDC.2016.107 Published online by Cambridge University Press

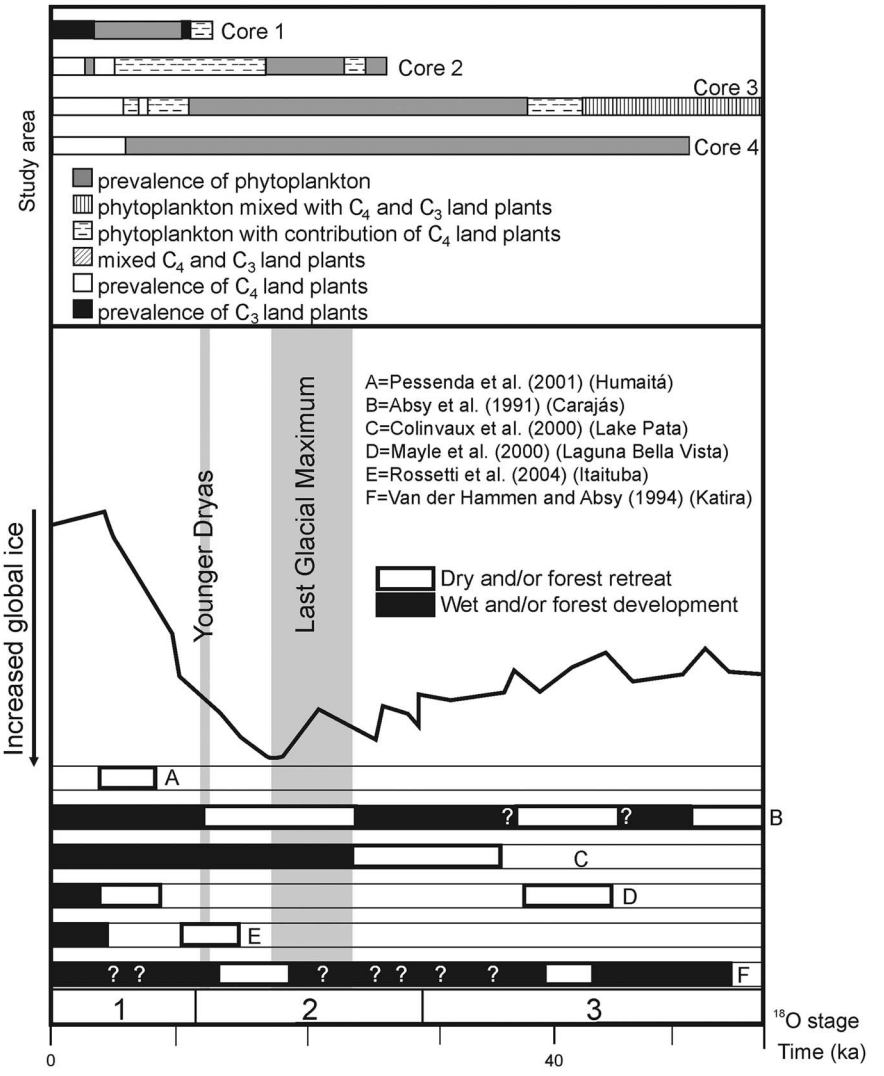

Figure 7 Types of organic matter preserved in the sedimentary deposits of the study area, contrasted to the history of global ice fluctuation since near the last glacial episode (i.e. ~60 ka ago) [see text for discussion; curve of global ice after Crowley and North (1991); $\delta^{18}O$ stages from Emiliani (1955) and Shackleton (1969); ages are in cal yr BP; figure modified from Rossetti et al. (2014)].

42.8–41.8 cal ka BP, it declined in energy, with alternating sand and mud deposition continuing up to 39.0–38.0 cal ka BP. A varied contribution of different types of organic matter was expected during the active and gradual phase of channel abandonment. This is due to the possibility of having various environments with diverse plant types cut by the channel along its drainage basin. Indeed, the high fluctuation of $\delta^{13}C$ from –28.2 to –20.2‰ and C/N from 4.6 to 16.7 recorded in the channel deposits at around 5.4 m depth in core 3 suggests a mixture of phytoplankton with C_3 and C_4 land plants (Figures 5 and 7). Despite frequent oscillations, the progressive increase in C/N values, accompanied by the enrichment in $\delta^{13}C$, are consistent with the increased contribution of C_4 land plants through time. The upward change from fluctuating

https://doi.org/10.1017/RDC.2016.107 Published online by Cambridge University Press

and higher $\delta^{15}N$ values into more uniform and lower values is in agreement with the presence of land plants.

Core 3 recorded also the time interval before 39.0–38.0 to 35.0–34.3 cal ka BP, when following a period of slowly declining energy, the channel became completely abandoned, as indicated by only mud settling from suspensions in low-energy environments (i.e. facies association FAC). Such an environmental context favors sediments with *in situ* organic matter. Thus, the sudden depletion in $\delta^{13}C$ and decrease in C/N during this time are consistent with the prevalence of freshwater phytoplankton in this initial phase of channel abandonment.

Considering the estimated sedimentation rate of 0.2 mm yr^{-1}, the two time ranges discussed above were also represented in the lower part of core 4. As in core 3, a channel interpretation for these temporally corresponding deposits was confirmed by the upward transition from facies associations FAA, FAB to FAC, indicative of decreasing flow energy with time. The sharp erosional base of FAA is compatible with a confined environment, typical of channels. Bedload transport within the active channel is recorded by the sandy deposits overlying the basal surface, and the cross-stratification indicates bedform migration at the channel bottom under low flow regime. Thus, sand started filling up a channel environment in core 4 just before ~40.0 cal ka BP, when the channel recorded at core 3 was already abandoned. Despite these differences in sedimentary facies, the isotope and C/N signals of these two sedimentary channel successions are comparable, confirming the increment of organic matter derived from phytoplankton after ~40.0 cal ka BP.

The interval between 26.0–25.5 and 22.1–21.6 cal ka BP is well represented in core 2, where the sedimentary record indicated the prevalence of mud deposition from suspensions in a low energy environment. The large volume of parallel-laminated mudstone formed during this time interval at this locality attests mud settling from suspensions, while the thin sandstone layers were due to episodes of relatively higher energy flows. The two coarsening-upward successions between 3 and 4 m in core 2 (Figure 4), suggestive of eventual flooding with development of crevasse splays, and the location of this core marginally to a paleomeander (core 2), support deposition in a floodplain and/or oxbow lake environments. While these floodplains were developing, the channel at core 4 became abandoned. This history is also represented in core 3, although a period of erosion and soil development (see 3.8 m depth in Figure 6) may have destroyed part of the sedimentary record at this locality. Independently of the dissimilar sedimentary history, these cores displayed analogous $\delta^{13}C$ and C/N trends that either remained with persistently depleted $\delta^{13}C$ and extremely low C/N values, or showed an upward trend into slight enrichment of $\delta^{13}C$ and higher C/N values. An exception is the lower part of core 2 between 8.0 and 7.2 m depth, where $\delta^{13}C$ was as depleted as –22.9‰, which may be related to an episodic higher contribution of land plants. It is interesting to note that the $\delta^{13}C$ values in this depth interval were more enriched than those recorded in leaves from the modern forest, which supports a slow increment in C_4 plants. It follows that the early phase of the LGM in southeastern Amazonia may have had flooded fluvial environments with organic matter derived mainly from phytoplankton, but with episodic contribution of probably C_4 land plants. The fact that the $\delta^{15}N$ values are mostly from 4.0 to nearly 8.0‰ is in agreement with aquatic plants, at the same time that its decrease to values as low as 2.6‰ between 8.0 and 7.2 m depth coincides with the suggested episodic contribution of C_4 land plants.

After ~22.0 cal ka BP, muddy deposition occurred in all cores. This is represented in core 4 by the complete channel abandonment. This phase is recorded by the upward gradation from FAA to FAB and then FAC, a sedimentary succession including heterolithic and muddy deposits

https://doi.org/10.1017/RDC.2016.107 Published online by Cambridge University Press

related to decreasing flows. Considering that the channel morphology is still preserved at the surface in this core, and also in core 3, the most likely hypothesis is that the essentially muddy deposits from the uppermost part of these successions (i.e. FAC) record oxbow lakes formed after channel abandonment. The soil profile at 1.4 m depth in core 3 indicates an episode of nondeposition and/or erosion. This event may have been local, as it was not recorded in core 4, which seems to record continuous sedimentation. The muddy deposits formed along core 1 and also after 22.0–21.6 cal ka BP in core 2 are thicker and probably record floodplains, which is suggested by their location in a young terrace close to the modern Madeira River (core 1) and marginally to a paleomeander (core 2).

The upward enrichment of $\delta^{13}C$, accompanied by higher C/N along the oxbow lake and floodplain deposits from the end of the LGM, suggests an increased contribution of C_4 land plants, particularly in the Holocene. Interestingly, this trend was recorded only in cores located where the modern landscape is also characterized by grassland and shrubland (i.e. cores 2, 3, and 4). In core 2, this trend was evidenced by an enrichment in $\delta^{13}C$ to –15.0‰, while the C/N, although still low, was increased to 11.3 at 5.3–5.5 cal ka BP. Following a short episode of very low C/N suggestive of phytoplankton, the trend to C_4 land plants was evidenced upward in this core by the highest C/N values of 37.6, with enriched $\delta^{13}C$ of 18.6‰; the $\delta^{15}N$ corresponding to this depth displayed a value (3.3‰) commonly related to terrestrial plants. The sudden increased contribution of C_4 land plants in core 3 may have occurred earlier, i.e. before 7.3–7.2 cal ka BP at ~1.2 m depth, when $\delta^{13}C$ varied from –20.9 to –16.9‰. However, the maximum C_4 contribution occurred at 1 m and above 0.2 m depths, when C/N values were higher, i.e. 11.5 and 12.2–12.1, respectively. A contribution of C_4 land plants was recorded also in core 4 before 2.3–2.2 cal ka BP (0.6–0.4 m depth), when $\delta^{13}C$ varied from –23.5 to –19.6 and then –12.7‰. The corresponding C/N variations from 4.4 to 9.1 and then 9.2 at these depths perhaps indicate the mixing of C_4 land plants with phytoplankton; the abrupt decrease in $\delta^{15}N$ is in agreement with these changes. The sudden C/N increase and $\delta^{13}C$ enrichment around the mid-Holocene may reflect C_4 grasses sourced either from land areas around the drainage basin or locally unflooded areas. Although C_3 grasses occur in the humid Amazonian lowland (e.g. Lima 2008), grasses from modern floodplains do have $\delta^{13}C$ values compatible with C_4 land plants (i.e. –12.0 to –15.0‰; cf. Victoria et al. 1992).

Different from the other cores, core 1 is located in an area with modern forest. This core, which has the highest sedimentation rate (i.e. up to 0.7 mm yr^{-1}), is interesting because it records the entire Holocene. An episode of increased concentration in C_3 vascular plants at an uncertain age before the Holocene is possibly represented by $\delta^{13}C$ as depleted as –30.1‰ at ~6.8 m depth (Figure 3); this suggested land plant influence is in agreement with the low $\delta^{15}N$ values of 1.3‰. However, the corresponding C/N was still low (i.e. up to 10.0), attesting phytoplankton, probably with some contribution of C_3 land plants (Figure 3) until ~11.1–10.7 cal ka BP, when the change into even lower C/N values suggests the increased contribution of phytoplankton. Only at ~3.4–3.1 cal ka BP the C/N slightly increased, probably due to the progressive contribution of C_3 land plants during the establishment of the overlying forested landscape. The soil profile dated at 6.5–6.3 cal ka BP recorded a local hiatus not recorded in any of the other cores.

Controls on Plant Distribution through Time: Climate Versus Sedimentary Dynamics

Despite the incomplete temporal record of individual sites, the studied cores represent an almost continuous testimony of sedimentation in southwestern Amazonia for most of the LG and also the Holocene. Thus, they provide significant data for reconstructing vegetation changes and analyzing the climate variations during this time.

https://doi.org/10.1017/RDC.2016.107 Published online by Cambridge University Press

Previous publications have considered two scenarios for explaining vegetation changes during the late Quaternary in Amazonia. The first scenario considers alternations from wet (warm) to dry (cold) periods mainly based on the presence/absence of forest and herb pollen (e.g. van der Hammen and Absy 1994; Behling and Hooghiemstra 1999; Behling and Costa 2000, 2001; Mayle et al. 2000; Haffer 2001; Sifeddine et al. 2001; van der Hammen 2001). The second paleoclimatic scenario depicts a relatively undisturbed Amazonian rainforest during the last 50,000 yr (e.g. Colinvaux et al. 1996, 2000, 2001; Bush et al. 2004; Irion et al. 2006; Mayle and Power 2008; Toledo and Bush 2008). Most of the available palynological data (Figure 7) indicate three episodes of savanna expansion in eastern Amazonia for the Late Pleistocene (i.e. >51.0 ^{14}C ka BP, 40.0 ^{14}C ka BP, and 23.0 – 11.0 ^{14}C ka BP) (Absy et al. 1991). The climate was wet in the Late Pleistocene before the LGM in Carajás (Absy et al. 1991), although a dry period was recorded in Laguna Bella Vista (Mayle et al. 2000). Although without a direct effect on the forest, Lake Pata also had the lowest lake level between 35 – 23 ^{14}C ka BP (Colinvaux et al. 2000). Forest was recorded in the Katira area in the State of Rondonia before 49.0 ^{14}C ka BP, with its replacement by savanna between 41.0 and 18.0 ^{14}C ka BP (van der Hammen and Absy 1994). In addition, paleontological (Webb and Rancy 1996; Vivo and Carmignotto 2004; Rossetti et al. 2004) and geological (Bibus 1983; Sifeddine et al. 2001) data suggest a Late Pleistocene climate drier than in the present.

The detailed analysis of isotope and C/N data and their distribution along the studied cores showed no clear record of plant types that could be related exclusively to arid climate before 39.0–38.0 cal ka BP. This timeframe is particularly well represented in cores 3 and 4, which were related to paleomeanders of the Madeira River. This river has a regional expression, being one of the most extensive Amazonian tributaries and the fifth longest river in the world. Thus, the organic matter content present in cores 3 and 4 may have reflected the overall floristic composition over a wide range of environments in the region, being useful for discussing the climate prevailing over this drainage basin. The prevalence of phytoplankton in cores 3 and 4 before 39.0 to 38.0 cal ka BP (Figure 7) may suggest a dominance of wet conditions with widespread flooded areas. The subordinate occurrence of C_4 land plants in these cores could signify that the overall wet period alternated with short dry episodes. This climatic interpretation for the study area is in good agreement with the prevalence of wet climate with short dry periods in the Katira site (van der Hammen and Absy 1994). It is also concordant with the alternation of forest and savanna proposed for the Carajás site (Absy et al. 1991) during this time interval. Interestingly, the clearest increase of C_4 land plants recorded around ~40.0 ka BP in the study area matches well with a dry phase in the Katira and Carajás sites, as well as in the Laguna Bella Vista (Mayle et al. 2000).

The climatic record between ~40 ka BP and the onset of the LGM in Amazonia is more variable, with sites such as Carajás, and probably also Katira, indicating wet conditions with forest expansion, while other areas, such as Lake Pata, recorded the lowest lake level related to a maximum dry phase, although without a clear effect in the rainforest (Colinvaux et al. 2000; Figure 7). In addition, following a dry phase just after 40.0 cal ka BP, Laguna Bella Vista also had a wet and warm climate, which would have favored the rainforest expansion (Mayle et al. 2000). Our data show deposits with a prevalence of phytoplankton after 38.0 cal ka BP, a trend that continued through the LGM. In addition, previously published pollen data from two of our studied cores (i.e. cores 1 and 2) point to wet, but cold-adapted, plants in association with herbs and tree taxa similar to modern ones at least between 42.6 and 35.2 cal ka BP (Cohen et al. 2014). These data are interesting because they suggest the continuing cold but humid conditions in this Amazonian region toward the onset of the LGM. When these cold-adapted plant species

https://doi.org/10.1017/RDC.2016.107 Published online by Cambridge University Press

disappeared from the study area remains to be determined, but they did not last until the Holocene (Cohen et al. 2014).

Another point of interest derived from our data is the lack of evidence indicating significant vegetation change from the time spanning the LGM. This could suggest the prevalence of aquatic plants as a reflex of a humid climate. While this interpretation is in agreement with the continuous wet climate proposed in Lake Pata (Colinvaux et al. 2000; Figure 7), it conflicts with the dry climate generally proposed for the Amazonian lowlands during this time. For instance, savanna expansion related to a dry climatic phase is recorded in the Carajás site between 23.0 and 11.0 ka BP (Absy et al. 1991) and in the Katira site between ~13.0 and 18.0 ka BP (van der Hammen and Absy 1994). In addition, the occurrence of a megafauna in central Amazonian was related to a dry climate at least between 15 and 11.3 ka BP (Rossetti et al. 2004). Taking these works into account, and also considering the increased contribution of C_4 land plants recorded in cores 1, 2, and 3 toward the end of the Late Pleistocene, we argue that the climate may have continued to be cold and humid through the LGM, but probably with episodic droughts towards the end of the period.

The intensified aridity reported until the end of the Late Pleistocene may have crossed the Late Pleistocene–Holocene boundary. However, although the contribution of C_4 land plants continued in the Holocene deposits of the study area, there is no evidence to sustain that the sudden increase in this plant type, reported in the uppermost parts of cores 2 to 4, resulted from intensified aridity. A line of evidence leads to suggest that the higher contribution in C_4 land plants in these cores is more likely a consequence of sedimentary processes associated with the fluvial dynamics. Firstly, these peaks of C_4 land plants were documented only in depositional sites having sediments confined to channel paleolandforms formed in a relatively recent geological time and which are currently covered by herbaceous fields; site 1, which is covered by forest, displayed an almost continuous record of C_3 land plants during almost the entire Holocene. It follows that the amplification of herbaceous fields may have occurred only over abandoned channel sites following their infilling, with the resulting sediments being subaereally exposed. Secondly, the modern landscape of cores 2 to 4 contains herbaceous fields despite their location in a tropical humid region, which means that the occurrence of herbs in the mid-Holocene is not necessarily related to dry phases. Thirdly, the peaks with increment of C_4 land plants recorded in the cores 2 to 4 were not coeval, being initiated before ~5.5 cal ka BP in core 2, ~7.5 cal ka BP in core 3, and ~2.5 cal ka BP in core 4. Fourth, these ages are also not synchronous with Holocene dry episodes previously proposed for Amazonian areas. For instance, it has been suggested that climate remained dry in this region only until the early to mid-Holocene (Sifeddine et al. 1994; Mayle et al. 2000; Mayle and Power 2008) (Figure 7). Other authors also claimed many fluctuations between dry and wet episodes from the early to mid-Holocene (Hughen et al. 2000; Lea et al. 2000; Pessenda et al. 2004, 2005), including data from southwestern Amazonia (Pessenda et al. 1998, 2001; Freitas et al. 2001), but not afterwards. A continuous rainforest was recorded since 7.9 ^{14}C ka BP in Caxiuanã (Behling and Costa 2000), 8.3 ^{14}C ka BP in Lake Calado (Behling et al. 2001), and 11.0 ka BP in Carajás (Absy et al. 1991) (Figure 7). In addition, Lake Pata (Colinvaux et al. 2000) and Lake Katira (van der Hammen and Absy 1994) recorded a wet period throughout the Holocene.

The foregoing discussion leads us to propose an alternative model to explain the peaks of C_4 land plants reported in cores 2 to 4. Rather than reflecting dry episodes, our data supports the development of herbaceous fields a few thousand years ago, with their maintenance in the modern landscape being due to the evolution of the fluvial system from river channels into oxbow lakes. As the river cut off took place, a change in the type of organic matter sourced into

this depositional system may have occurred. River deposits generally have greater potential to record pollen transported through the drained area, while lake deposits contain organic matter derived from freshwater phytoplankton. Thus, the widespread development of water bodies along floodplains would have resulted in higher phytoplankton production. However, as the lakes were abandoned, the sedimentary deposits exposed to the surface were colonized by herbs. This condition remained up to the present probably due to the maintenance of the water table close to the surface at least during a great part of the year in this wetland.

Therefore, the modern herbaceous fields in the study area could not be linked to past dry climates. The fact that this plant type is confined to paleomorphologies representative of depositional sites that remained active until the Holocene (Figure 2) is consistent with its attribution to sedimentary dynamics as the most likely explanation. This interpretation is also favored because of the overall trend into increased humidity up to 40% after the Young Dryas (Maslin and Burns 2000), and particularly after the mid-Holocene, when the rainforest spread out over the Amazonian lowland (Sifeddine et al. 2001; Rossetti et al. 2005).

CONCLUSIONS

This survey integrating $\delta^{13}C$ and C/N analyses with sedimentology and ^{14}C chronology was successful for reconstituting changes in vegetation patterns in southwestern Amazonia during the late Quaternary. In addition, despite the limitations due to uncertainties in the fixation mechanisms during nitrogen fractionation pathways, the $\delta^{15}N$ values were also generally fairly consistent with C/N variations; thus, they helped the differentiation between organic matter derived from aquatic and land plants. We concluded that the climate was wet with short dry episodes before ~40 cal ka BP. From this time up to the onset of the LGM, humid and cold climate prevailed, with intensified aridity toward the end of the Late Pleistocene. Although this trend continued into the Holocene, the peaks of increased C_4 land plant contribution recorded at 5.5 cal ka BP in core 2, ~7.5 cal ka BP in core 3, and ~2.5 cal ka BP in core 4, and the maintenance of herbaceous fields in the modern landscapes of these sites, are related to sedimentary processes due to fluvial dynamics, rather than intensified aridity. Thus, the late Holocene climate was humid, which favored the expansion of the Amazonian rainforest as we see today. The abandonment of channel and lake environments would have favored subaerial exposure and soil development, creating sites favorable for the colonization of herbs of C_4 photosynthetic pathway. It follows that great care must be taken when using changes in plant communities for paleoclimatic purpose, as factors other than climate, such as depositional processes, must be also regarded.

ACKNOWLEDGMENTS

This work was financially supported by the Brazil's National Council for Scientific and Technological Development-CNPq (#471483/06-0) and #550331/2010-7 and Research Funding Institute of the State of São Paulo-FAPESP (#13/50475-5). The authors acknowledge the logistic support of the Brazilian Geological Survey-CPRM and the Santo Antonio Hydroelectric during field campaigns. Dr Peter Langdon, as well as two anonymous reviewers, contributed with numerous suggestions and corrections that helped to significantly improve an early version of the manuscript.

SUPPLEMENTARY MATERIAL

To view supplementary material for this article, please visit https://doi.org/10.1017/RDC.2016.107

REFERENCES

Absy ML, Cleef A, Fournier M, Martin L, Servant M, Sifeddine A, Silva F, Soubié F, Suguio K, Turcq B, van der Hammen T. 1991. Mise en évidence de quatre phases d´ ouverture de la forêt dense dans le sud-est de L'Amazonie au tours des 60.000 dernières années. Première comparaison avec d´autres régions tropicales. *Comptes Rendus de l´Académie des Sciences Paris (Series II)* 312: 673–8.

Adams JM, Faure H, Faure-Denard L, McGlade M, Woodward FI. 1990. Increases in terrestrial carbon storage from the last glacial maximum to the present. *Nature* 348(6303):711–4.

Amorim MA, Moreira-Turcq PF, Turcq BJ, Cordeiro RC. 2009. Origem e dinâmica da deposição dos sedimentos superficiais na Várzea do Lago Grande de Curuai, Pará, Brasil. *Acta Amazonica* 39:165–72.

Atchley SC, Nordt LC, Dworkin SI. 2004. Eustatic control on alluvial sequence stratigraphy: a possible example from the Cretaceous–Tertiary transition of the Tornillo Basin, Big Bend National Park, west Texas, USA. *Journal of Sedimentary Research* 74(3):391–404.

Behling H. 1996. First report on new evidence for the occurrence of Podocarpus and possible human presence at the mouth of the Amazon during the late-glacial. *Vegetation History and Archaeobotany* 5(3):241–6.

Behling H, Costa ML. 2000. Holocene environmental changes from the Rio Curuá record in the Caxiuanã region, eastern Amazon Basin. *Quaternary Research* 53(3):369–77.

Behling H, Costa ML. 2001. Holocene vegetational and coastal environmental changes from the Lago Crispim record in northeastern Pará State, eastern Amazonia. *Reviews of Palaeobotany and Palynology* 114(3–4):145–55.

Behling H, Hooghiemstra H. 1999. Environmental history of the Colombian savannas of the Llanos Orientales since the Last Glacial Maximum form lake records El Pinal and Carimagua. *Journal of Paleolimnology* 21(4):461–76.

Behling H, Keim G, Irion G, Junk W, Mello JAN. 2001. Holocene environmental changes in the central Amazon Basin inferred from Lago Calado (Brazil). *Palaeogeography, Palaeoclimatology, Palaeoecology* 173:87–101.

Bibus E. 1983. Die klimamorphologische Bedeutung von stone-lines und Decksedimenten in mehrgliedrigen Bodenprofilen Brasiliens. *Zeitschrift für Geomorphogie* 48:79–98.

Burbridge RE, Mayle FE, Killeen TJ. 2004. Fifty-thousand year vegetation and climate history of Noel Kempff Mercado National Park, Bolivian Amazon. *Quaternary Research* 61:215–30.

Bush MB, Weimann M, Piperno DR, Liu KK-B., Colinvaux PA. 1990. Pleistocene temperature depression and vegetation change in Ecuadorian Amazonia. *Quaternary Research* 34:330–45.

Bush MB, Miller MC, Oliveira PE, Colinvaux PA. 2000. Two histories of environmental change and human disturbance in eastern lowland Amazonia. *The Holocene* 10:543–54.

Bush MB, Oliveira PE, Colinvaux PA, Miller MC, Moreno JE. 2004. Amazonian palaeoecological histories: One Hill, Three Watersheds. *Palaeogeography, Palaeoclimatology, Palaeoecology* 214:359–93.

Carneiro Filho A, Schwartz D, Tatumi SH, Rosique T. 2002. Amazonian paleodunes provide evidence for drier climate phases during the Late Pleistocene–Holocene. *Quaternary Research* 58:205–9.

Chen F, Zhang L, Yang Y, Zhang D. 2008. Chemical and isotopic alteration of organic matter during early diagenesis: evidence from the coastal area off-shore the Pearl River estuary, south China. *Journal of Marine Systems* 74:372–80.

Chikaraishi Y, Naraoka H. 2006. Carbon and hydrogen isotope variant of plant biomarkers in a plant-soil system. *Chemical Geology* 231:190–7.

Cloern JE, Canuel EA, Harris D. 2002. Stable carbon and nitrogen isotope composition of aquatic and terrestrial plants of the San Francisco Bay estuarine system. *Limnology and Oceanography* 47:713–29.

Cohen MCL, Rossetti DF, Pessenda LCR, Friaes YS, Oliveira PE. 2014. Late Pleistocene glacial forest of Humaitá-western Amazônia. *Palaeogeography, Palaeoclimatology, Palaeoecology* 415:37–47.

Colinvaux PA, Oliveira PE, Moreno JE, Miller MC, Bush MB. 1996. A long pollen record from lowland Amazonia: forest and cooling in glacial times. *Science* 274:85–8.

Colinvaux PA, Oliveira PE, Bush MB. 2000. Amazonian and neotropical plant communities on glacial time-scales: the failure of the aridity and refuge hypotheses. *Quaternary Science Reviews* 19: 141–69.

Colivaux PA, Irion G, Räsänen ME, Bush MB, Mello JASN. 2001. A paradigm to be discarded: geological and paleoecological data falsify the Haffer and Prance refuge hypothesis of Amazonian speciation. *Amazoniana* 16:609–46.

Craine JM, Brookshire ENJ, Cramer MD, Hasselquist NJ, Koba K, Marin-Spiotta E, Wang L. 2015. Ecological interpretations of nitrogen isotope rations of terrestrial plants and soils. *Plant Soil* 396:1–26.

Crowley TJ, North GR. 1991. *Paleoclimatology*. Oxford: Oxford University Press.

Cunha PRC, Gonzaga FG, Coutinho LFC, Feijó FJ. 1994. Bacia do Amazonas. *Boletim de Geociências da Petrobras* 8:47–55.

Deines P. 1980. The isotopic composition of reduced organic carbon. In: Fritz P, Fontes JC, editors. *Handbook of Environmental Isotope Geochemistry*. New York: Elsevier. p 329–406.

Diefendorf AF, Freeman KH, Wing SL, Graham HV. 2011. Production of n-alkyl lipids in living plants

and implications for the geologic past. *Geochimica et Cosmochimica Acta* 75:7472–85.

Duarte L. 2003. Paleoflórula. In: Rossetti DF, Góes AM, editors. *O Neógeno da Amazônia Oriental*. Belém: Museu Paraense Emílio Goeldi Press. p 169–96.

Emiliani C. 1955. Pleistocene temperatures. *Journal of Geology* 63:538–78.

Francisquin MI, Lima CM, Pessenda LCR, Rossetti DF, França MC, Cohen MCL. 2014. Relation between carbon isotopes of plants and soils on Marajó Island, a large tropical island: implications for interpretation of modern and past vegetation dynamics in the Amazon region. *Palaeogeography, Palaeoclimatology, Palaeoecology* 415:91–104.

Freitas HA, Pessenda LCR, Aravena R, Gouveia SEM, Ribeiro AS, Boulet R. 2001. Late Quaternary vegetation dynamics in the southern Amazon Basin inferred from carbon isotopes in soil organic matter. *Quaternary Research* 55: 39–46.

Garcin Y, Shcefub E, Schwab VF, Garreta V, Gleixner G, Vincens A, Todou G, Séné O, Onana J-M, Achoundong G, Sachse D. 2014. Reconstructing C_3 and C_4 vegetation cover using n-alkane carbon isotope rations in recent lake sediments from Cameroon, Western Central Africa. *Geochimica et Cosmochimica Acta* 142:482–500.

Haffer J. 1969. Speciation in Amazonian forest birds. *Science* 165:131–7.

Haffer J. 2001. Hypotheses to explain the origin of species in Amazonia. In: Vieira IC, Silva JMC, Oren DC, D'Incao MA, editors. *Diversidade Biológica e Cultural da Amazônia*. Belém: Museu Paraense Emílio Goeldi Press. p 45–118.

Hughen KA, Southon JR, Lehman SJ, Overpeck JT. 2000. Synchronous radiocarbon and climate shifts during the last deglaciation. *Science* 290:1951–4.

Irion G, Bush MB, Mello JAN, Stüben D, Neumann T, Müller RG, Moraes JO, Junk JW. 2006. A multiproxy palaeoecological record of Holocene lake sediments from the Rio Tapajós, eastern Amazonia. *Palaeogeography, Palaeoclimatology, Palaeoecology* 240:523–36.

Keil RG, Tsamakis E, Fuh CB, Giddings JC, Hedges JI. 1994. Mineralogical and textural controls on organic composition of coastal marine sediments: hydrodynamic separation using SPLITT fractionation. *Geochimica et Cosmochimica Acta* 57: 879–93.

Lamb AL, Wilson GP, Leng MJ. 2006. A review of coastal palaeoclimate and relative sea-level reconstructions using $\delta^{13}C$ and C/N ratios in organic material. *Earth-Science Reviews* 75: 29–57.

Latrubesse EM, Franzinelli E. 2005. The late Quaternary evolution of the Negro River, Amazon, Brazil: implications for island and floodplain formation in large anabranching tropical systems. *Geomorphology* 70:372–97.

Lea DW, Pak DK, Spero HL. 2000. Climate impact of Late Quaternary, equatorial Pacific sea surface temperature variations. *Science* 289:1719–24.

Ledru M-P. 2002. Late Quaternary history and evolution of the cerrados as revealed by palynological records. In: Oliveira PS, Marquis RJ, editors. *The Tropical Cerrados of Brazil: Ecology and Natural History of a Neotropical Savanna*. New York: University Press. p 33–52.

Ledru M-P, Ceccantini G, Gouveia SEM, López-Sáez JA, Pessenda LCR, Riberito AS. 2006. Millennial-scale climatic and vegetation changes in a northern Cerrado (Northeast, Brazil) since the Last Glacial Maximum. *Quaternary Science Reviews* 25:1110–26.

Lima CM. 2008. Dinâmica da vegetação e inferências climáticas no Quaternário Tardio na região da Ilha de Marajó (PA), empregando os isótopos do carbono (^{12}C,^{13}C,^{14}C) da matéria orgânica de solos e sedimentos [PhD dissertation]. São Paulo: Universidade de São Paulo.

Liu KB, Colinvaux PA. 1985. Forest changes in the Amazon Basin during the last glacial maximum. *Nature* 318:556–7.

Magnusson WE, Sanaiotti TM, Lima AP, Martinelli LA, Victoria RL, Araújo MC, Albernaz AL. 2002. A comparison of $\delta^{13}C$ ratios of surface soils in savannas and forests in Amazonia. *Journal of Biogeography* 29:857–66.

Martin L, Fournier M, Mourguiart P, Sifeddine A, Turcq B, Absy ML, Flexor J-M. 1993. Southern oscillation signal in South American paleoclimatic data of the last 7000 years. *Quaternary Research* 39:338–46.

Martin L, Bertaux J, Correge T, Ledru M-P, Mourguiart P, Sifeddine A, Soubiès F, Wirrmann D, Suguio K, Turcq B. 1997. Astronomical forcing of contrasting rainfall changes in tropical South America between 12,400 and 8800 cal yr BP. *Quaternary Research* 47:117–22.

Maslin MA, Burns SJ. 2000. Reconstruction of the Amazon Basin effective moisture availability over the past 14,000 years. *Science* 290:2285–7.

Mayle FE, Power MJ. 2008. Impact of a drier Early–Mid-Holocene climate upon Amazonian forests. *Philosophical Transactions of the Royal Society B* 363:1829–38.

Mayle FE, Burbridge R, Killeen TJ. 2000. Millennial-scale dynamics of southern Amazonian rain forests. *Science* 290:2291–4.

McLaurin BT, Steel RJ. 2007. Architecture and origin of an amalgamated fluvial sheet sand, lower Castlegate Formation, Book Cliffs, Utah. *Sedimentary Geology* 197:291–311.

Meyers PA. 1994. Preservation of elemental and isotopic source identification of sedimentary organic matter. *Chemical Geology* 114:289–302.

Meyers PA. 1997. Organic geochemical proxies of paleoceanographic, paleolimnologic, and paleoclimatic processes. *Organic Geochemistry* 27: 213–50.

Ogrinc N, Fontolanb G, Faganelic J, Covellib S. 2005. Carbon and nitrogen isotope compositions of organic matter in coastal marine sediments (the Gulf of Trieste, N Adriatic Sea): indicators of sources and preservation. *Marine Chemistry* 95:163–81.

Ometto J, Ehleringer JR, Domingues TF, Berry JA, Ishida FY, Mazzi E, Higucji N, Flanagan LB, Nardoto GB, Martinelli LZ. 2006. The stable carbon and nitrogen isotopic composition of vegetation in tropical forests of the Amazon Basin, Brazil. *Biogeochemistry* 79:251–74.

Pessenda LCR, Gomes BM, Aravena R, Ribeiro AS, Boulet R, Gouveia SEM. 1998. The carbon isotope record in soils along a forest-cerrado ecosystem transect: implications for vegetation changes in the Rondônia State, southwestern Brazilian Amazon region. *The Holocene* 8: 599–603.

Pessenda LCR, Boulet R, Aravena R, Rosolen V, Gouveia SEM, Ribeiro AS, Lamotte M. 2001. Origin and dynamics of soil organic matter and vegetation changes during the Holocene in a forest-savanna transition zone, Brazilian Amazon Region. *The Holocene* 11:250–4.

Pessenda LCR, Ribeiro AS, Gouveia SE, Aravena R, Boulet R, Bendassoli JÁ. 2004. Vegetation dynamics during the late Pleistocene in the Barreirinhas region, Maranhão State, Northeastern Brazil, based on carbon isotopes in soil organic matter. *Quaternary Research* 62:183–93.

Pessenda LCR, Ledru MP, Gouveia SEM, Aravena R, Ribeiro AS, Bendassolli JA, Boulet R. 2005. Holocene palaeoenvironmental reconstruction in northeastern Brazil inferred from pollen, charcoal and carbon isotope records. *The Holocene* 15: 814–22.

Premuzic ET, Benkovitz CM, Gaffney JS, Walsh JJ. 1982. The nature and distribution of organic matter in the surface sediments of world oceans and seas. *Organic Geochemistry* 4:63–77.

Radambrasil. 1978. Folha SB.20 Purus-Geologia. *Departamento Nacional de Pesquisas Minerais* 17:19–128.

Reimer PJ, Bard E, Bayliss A, Beck JW, Blackwell PG, Ramsey CB, Buck CE, Cheng H, Edwards RL, Friedrich M, Grootes PM, Guilderson TP, Haflidason H, Hajdas I, Hatté C, Heaton TJ, Hoffmann DL, Hogg AG, Hughen KA, Kaiser KF, Kromer B, Manning SW, Reimer MRW, Richards DA, Scott EM, Southon JR, Staff RA, Turney CSM, van der Plicht J. 2013. IntCal13 and Marine13 radiocarbon age calibration curves 0–50,000 years cal BP. *Radiocarbon* 55(4): 1869–87.

Rommerskiechen F, Eglinton G, Dupont L, Rullkötter J. 2006. Glacial/interglacial changes in southern Africa: compound-specific $\delta^{13}C$ land plant biomarker and pollen records from southeast Atlantic continental margin sediments. *Geochemistry, Geophysics, Geosystems* 6:QO8010.

Rossetti DF, Toledo PM, Moraes–Santos HM, Santos AEA Jr. 2004. Reconstructing habitats in Central Amazonia using megafauna, sedimentology, radiocarbon and isotope analysis. *Quaternary Research* 61:289–300.

Rossetti DF, Toledo PM, Góes AM. 2005. New geological framework for Western Amazonia (Brazil) and implications for biogeography and evolution. *Quaternary Research* 63:78–89.

Rossetti DF, Cohen MCL, Bertani TC, Hayakawa EH, Paz JDS, Castro DF, Friaes Y. 2014. Late Quaternary fluvial terrace evolution in the main southern Amazonian tributary. *Catena* 116: 19–37.

Sandweiss DH, Richardson JBI, Reitz EJ, Rollins HB, Maasch KA. 1996. Geoarchaeological evidence from Peru for a 5000 years BP. *Onset of El Nino. Science* 273:1531–3.

Sandweiss DH, Maasch KA, Anderson DG. 1999. Climate and culture: transitions in the Mid-Holocene. *Science* 283:499–500.

Schwab VF, Garcin Y, Sachse D, Todou G, Séné O, Onana J-M, Achoundong G, Gleixner G. 2015. Effect of aridity on $\delta^{13}C$ and δD values of C_3 plant- and C_4 graminoid-derived leaf wax lipids from soils along an environmental gradient in Cameroon (Western Central Africa). *Organic Geochemistry* 78:99–109.

Servant M, Fontes J-C, Rieu M, Saliège X. 1981. Phases climatiques arides holocènes dans le sud-ouest de l'Amazonie (Bolivie). *Comptes Rendus de l´Académie des Sciences Paris Series II* 292: 1295–7.

Shackleton NJ. 1969. The last interglacial in the marine and terrestrial records. *Proceedings of the Royal Society of London B* 174:135–54.

Sinninghe Damsté JS, Vershuren D, Ossebaar J, Blokker J, van Houten R, van der Meer MT, Plessen B, Schouten S. 2011. A 25,000-year record of climate-induced changes in lowland vegetation of eastern equatorial Africa revealed by the stable carbon-isotopic composition of fossil plant leaf waxes. *Earth and Planetary Science Letters* 302:236–46.

Sifeddine A, Bertand P, Founier L, Servant M, Soubies F, Suguio K, Turcq B. 1994. The lacustrine organic sedimentation in tropical humid environment (Carajás, eastern Amazonia, Brazil)—relationship with climatic changes during the last 60,000 years BP. *Bulletin de la Société Géologique de France* 165:613–21.

Sifeddine A, Marint L, Turcq B, Volkmer–Ribeiro C, Soubiès F, Cordeiro RC, Suguio K. 2001. Variations of the Amazonian rainforest environment: a sedimentological record covering 30,000 years. *Palaeogeography, Palaeoclimatology, Palaeoecology* 168:221–35.

Stuiver M, Polach HA. 1977. Discussion: reporting of ^{14}C data. *Radiocarbon* 19(3):355–63.

Teeuw RM, Rhodes EJ. 2004. Aeolian activity in northern Amazonia: optical dating of Late

Pleistocene and Holocene paleodunes. *Journal of Quaternary Science* 19:49–54.

Thornton SF, McManus J. 1994. Applications of organic carbon and nitrogen stable isotope and C/N ratios as source indicators of organic matter provenance in estuarine systems: evidence from the Tay Estuary, Scotland. *Estuarine, Coastal and Shelf Science* 38:219–33.

Toledo MB, Bush MB. 2008. A Holocene pollen record of savanna establishment in coastal Amapá. *Anais da Academia Brasileira de Ciências* 80:341–51.

van der Hammen T. 2001. Paleoecology of Amazônia. In: Vieira IC, Silva JMC, Oren DC, D´Incao MA, editors. *Diversidade Biológica e Cultural da Amazônia*. Belém: Museu Paraense Emílio Goeldi Press. p 19–44.

van der Hammen T, Absy ML. 1994. Amazonia during the last glacial. *Palaeogeography, Palaeoclimatology, Palaeoecology* 109:247–61.

van der Hammen T, Hooghiemstra H. 2000. Neogene and Quaternary history of vegetation, climate and plant diversity in Amazonia. *Quaternary Science Reviews* 19:725–42.

Victoria RL, Martinelli LA, Trivelin PCO, Matsui E, Forsberg BR, Richey JE, Devol AL. 1992. The use of stable isotopes in studies of nutrient cycling: carbon isotope composition of Amazon varzea sediments. *Biotropica* 24:240–9.

Vitousek PM, Menge DN, Reed SC, Cleveland CC. 2013. Biological nitrogen fixation: rates, patterns and ecological controls in terrestrial ecosystems. *Philosophical Transactions of the Royal Society B: Biological Science* 368:2013.

Vivo M, Carmignotto AP. 2004. Holocene vegetation change and the mammal faunas of South America and Africa. *Journal of Biogeography* 31:943–57.

Wang L, Macko SA. 2011. Constrained preferences I nitrogen uptake across plant species and environments. *Plan, Cell & Environment* 34:525–34.

Webb SD, Rancy A. 1996. Late Cenozoic Evolution of Neotropical Mammal Fauna. In: Jackson JBC, Budd AB, Coates AG, editors. *Evolution and Environment in Tropical America*. Chicago: University of Chicago Press. p 335–58.

Weng C, Bush MB, Athens JS. 2002. Two histories of climate change and hydrarch succession in Ecuadorian Amazonia. *Review of Palaeobotany and Palynology* 120:73–90.

Wilson GP, Lamb AL, Leng MJ, Gonzalez S, Huddart D. 2005. Variability of organic $\delta^{13}C$ and C/N in the Mersey Estuary, U.K. and its implications for sea-level reconstruction studies. *Estuarine, Coastal and Shelf Science* 64:685–98.

https://doi.org/10.1017/RDC.2016.107 Published online by Cambridge University Press